Stochastic Modeling of a Memory-Assisted Measurement-Device-Independent Quantum Key Distribution System in Free-Space Metropolitan Environments

Fares Nada, Student Member, IEEE, Amber Hussain, Tasmi R. Ahmed, and Connor Kupchak, Member, IEEE

Abstract—On the pathway to quantum key distribution on a global scale, will be the realization of metropolitan-sized Memory Assisted Measurement-Device-Independent Quantum Key Distribution (MA-MDI-QKD) systems. Here, we present a simplistic and intuitive stochastic model to predict key distribution rates in a MA-MDI-QKD scheme that addresses the realworld parameters inherent to free-space quantum communication channels. Specific to our algorithm, the memory-assisted based system allows us to leverage the advantage of asynchronously loaded quantum memory when predicting the distribution rates. Specifically, by focusing on metropolitan distances, we perform simulations tailored toward a system based on free-space links and field-deployable quantum memory. We show the capabilities of our model to predict key rate distributions over ranges of 10-50 km for a set of atmospheric-based parameters and selection of QM efficiencies and coherence times. This tool provides impactful insights into the deployment and optimization of practical MA-MDI-QKD networks in urban environments. Our streamlined approach is a valuable addition to existing quantum network simulators for the smooth integration of quantum networking into the field of communications engineering.

Index Terms—quantum key distribution, quantum network modeling, device independent key distribution, quantum memory

I. INTRODUCTION

ROR the past decades, quantum key distribution (QKD) has been recognized as the global solution to exchange cryptographic keys for security fully guaranteed. From its infancy, BB84 [1] has been celebrated as a full-proof solution for distributing symmetric encryption keys. However, BB84 encounters a number of practical challenges that can hinder its real-world application. These include detector imperfections, the need for idealized quantum sources and the degradation of key rate with optical loss [2]. More recently, a enhanced quantum key distribution scheme was introduced that is intrinsically secure against detector side-channel attacks, known as measurement-device-independent QKD (MDI-QKD) [3], [4]. The concept of MDI-QKD stems from performing a time-reversed version of entanglement-based QKD [5]. Achieving a secret key rate in MDI-QKD, requires performing a Bell state measurement (BSM) at an intermediate node between

parties (conventionally named Charlie) to signal entanglementtype correlations between the communicating parties, namely Alice and Bob.

In such a scheme, the secrecy of the key rate is robust against the situation where Charlie, and the intermediate node itself, cannot be trusted or acts as an eavesdropper. Here, no assumptions about the quality of the measurement apparatus are required, and the net result is a scheme providing enhanced security as compared to traditional QKD. Soon after the concept was first introduced [3], the experimental demonstrations of MDI-QKD were soon reported [6].

Transitioning these lab-based demonstrations into real-world environments, requires another level of innovation. Many facets will be required including use of metropolitan fibre networks, integration of QKD hardware into communications server rooms, as well as the progression in technology to make the hardware capable of mass production and economic feasibility. As such, the first step to achieving globally connected QKD networks will be their establishment at metropolitan distances [7]. Over the past decade, there have now been numerous demonstrations of quantum communications in real-world settings [8], [9], including MDI-QKD [10], [11] and very recently MA-MDI-QKD [12].

Traditionally, quantum communication implementations are undertaken in fibre-based networks [13]. However, fibre systems can be limited by fixed propagation loss and birefringence effects. Hence, inclusion of transmission over free space is also being heavily pursued [14], [15]. Furthermore, a global QKD network would necessitate satellite-based systems. Free-space optical transmission comes with a different set of challenges [16] including atmospheric turbulence [17] and the need for adaptive optics [18] and beam tracking [15].

Predictive models for city-scale MDI-QKD schemes will be vital as these network become established in our communication infrastructures. Here, we present a transformative stochastic modeling algorithm based on Monte Carlo sampling that allows the prediction of key rates using a MA-MDI-QKD system over metropolitan distances. We incorporate many of the effects that will need consideration in urban-based MA-MDI-QKD systems and introduce ways to stochastically model QM-based parameters. Our algorithm is intuitive in nature and serves as a simple, open source scheme that augments to the current family of quantum network simulators [19].

F. Nada is with Department of Electronics, Carleton University, Ottawa, Canada (e-mail: faresnada@cmail.carleton.ca).

A. Hussain is with Department of Electronics, Carleton University, Ottawa, Canada (e-mail: amberhussain@cmail.carleton.ca).

T. R. Ahmed is with Department of Electronics, Carleton University, Ottawa, Canada (e-mail: tasmiahmed@cmail.carleton.ca).

C. Kupchak is with Department of Electronics, Carleton University, Ottawa, Canada (e-mail: connorkupchak@cunet.carleton.ca).

II. MEMORY-ASSISTED MDI-QKD

Extending the MDI-QKD protocol to include quantum memories retains the original benefits of the protocol while also providing added advantages over traditional MDI-QKD. Foremost, is the ability to handle the asynchronous arrival of Alice and Bob's quantum qubits at the central node. As such, the transmission channel scaling improves from approximately, $\sim \mathcal{O}(\eta_t)$ to $\sim \mathcal{O}(\sqrt{\eta_t})$, significantly enhancing distribution rates over long distances.

MA-MDI-QKD shares similarities with a single-node quantum repeater. Here, two quantum memories, one allocated to each of Alice and Bob, are located at an intermediary station hosted by Charlie as illustrated in Fig. 1. In its most basic implementation, each user transmits a photonic qubit encoded in one of the four BB84 states toward this intermediate station. These qubits are subsequently stored in each user's dedicated QM.

Once both QMs hold quantum states from their respective users, whether loaded synchronously or asynchronously, the stored states are simultaneously retrieved to undergo a Bell State Measurement. This process results in correlated keys exclusive to the participating users. For MA-MDI-QKD to be successful, the QMs employed in this system need to satisfy specific requirements including suitable read-in and read-out times, high indistinguishability and a sufficiently low QM noise floor.

To begin, we delineate the information-based steps of the MA-MDI-QKD protocol with polarization qubits.

1) Alice and Bob each randomly prepare one of four polarization encoded qubit states:

$$\left|\psi\right\rangle =\left\{ \left|H\right\rangle ,\left|V\right\rangle ,\left|+\right\rangle ,\left|-\right\rangle \right\}$$

where

$$|+\rangle = \frac{1}{\sqrt{2}}(|H\rangle + |V\rangle) \quad |-\rangle = \frac{1}{\sqrt{2}}(|H\rangle - |V\rangle).$$

The set $\{|H\rangle\,,|V\rangle\}$ represents qubits corresponding to horizontal $(|H\rangle)$ and vertical $(|V\rangle)$ polarization respectively and will be referred to as the Z-basis (rectilinear). The set $\{|+\rangle\,,|-\rangle\}$ will be referred to as the X-basis (diagonal). Note that this first stage is identical to the traditional BB84 protocol [1]. Alice and Bob will both record their sent qubits before transmitting via quantum channel to the intermediate station hosted by the third party Charlie. A QM dedicated to each of Alice and Bob's channels is situated at this intermediate station.

- 2) Once both QMs have successfully loaded a quantum state, synchronously or asynchronously, both states are retrieved from the QM to undergo a subsequent Bell State measurement. The outcome of the BSM is communicated by Charlie back to Alice or Bob (or both). If the BSM is successful, Alice and Bob will either preserve or flip the recorded bits in their raw data. However, if the measurement fails, both Alice and Bob discard their bits and the procedure begins again at Step 1.
- When a sufficient amount of bits have been successfully generated via communication from the central station,

- Alice and Bob can terminate the protocol. Next, they communicate their basis choices (Z or X) over a classical channel as shown in Fig. 1. To ensure correlated key bits, only the attempts where they used the same basis to generate their respective states are used; thus both parties can now share a common key length.
- 4) In line with BB84 protocols, the final step involves classical QKD post-generation processing composed of error correction and privacy amplification techniques to ensure the secrecy of the shared key.

These steps describe how Alice and Bob can perform a QKD protocol that is robust against imperfect measurement apparatus and an untrusted central node (Charlie). The second step above describes where the enhanced benefit of quantum memories factor in. The QMs allow for the asynchronous arrival of qubits from Alice and Bob which can allow for a MA-MDI-QKD protocol to surpass a purely synchronous MDI-QKD scheme. Since a BSM apparatus requires simultaneous arrival of both qubits to perform a reliable measurement. Many attempts can be discarded due to the requirement of near-perfect timing correlation for arrival of the qubits to the central station leading to resource inefficiencies.

MDI-QKD protocols hold inherent advantages over direct BB84 transmission. Among these, MDI-QKD systems do not rely on trust in the measurement devices used, which is an assumption needed in BB84. If an eavesdropper (hereafter referred to as Eve) has access to the measurement devices in BB84, this in conjunction with the bases choice communication between Alice and Bob, will allow Eve to obtain information about Alice and Bob's secret key. However, in MDI-QKD, even if Eve controls the BSM setup, she will not be able to obtain the secret key since the BSM only shows the nature of the correlation between Alice and Bob's qubits without revealing their actual states. The core of the BSM detecting a two-photon interference effect is a vital characteristic for the signal to be distinguished from background noise, particularly over long distances.

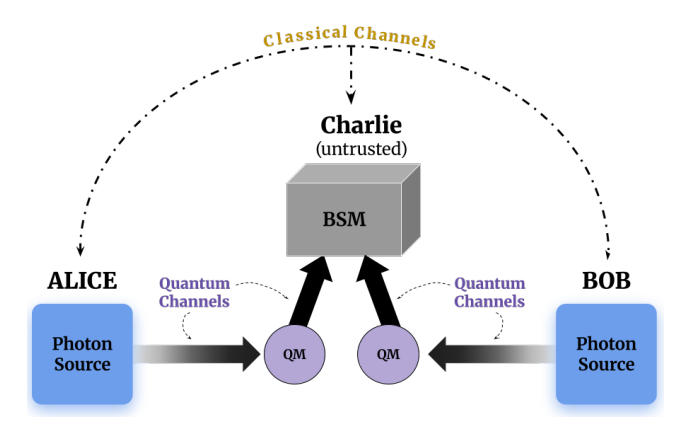


Fig. 1. Scheme of a measurement-device-independent quantum repeater where QMs are utilized. The core process involves a BSM on qubits originating from two separate sources, which can be generated from either single-photon states or weak coherent pulses.

III. ANALYTICAL KEY RATE ANALYSIS

Calculation of MA-MDI-QKD key generation rate requires consideration of numerous factors. In the MDI-QKD schemes, the qubit sources held by Alice and Bob in Fig. 1 are often one of two main types: a single photon source (SPS) or weak coherent pulses (WCP). A perfect SPS generates pure single photons in a desired spatiotemporal mode. However, engineering of such an idealized source presents many difficulties. Hence, many real-world systems key distribution systems instead employ WCP which are faint laser pulses with photon numbers following a Poisson distribution based on state amplitude. With WCP some pulses may contain more than one photon or even none at all. As such, implementations with WCP require additional considerations when calculating key rates due to the distribution of photon number. In our treatment, we will investigate the use of both SPS and WCP sources and how they translate to the distribution rates in a MA-MDI-QKD setup.

A. Rates using single photon states

When modeling assuming a SPS, the key rate will be calculated using Eq. 1. This rate consists of three primary elements: total gain, error rate and the cost of error correction. expressed as follows [20]:

$$R_{corr} = Q[1 - fh(QBER)]. \tag{1}$$

Where:

- R: Error corrected key generation rate
- Q: Total Gain (probability of detecting a signal)
- f: error correction efficiency, taken to be 1 here
- h(QBER): binary entropy function of QBER (Quantum Bit Error Rate)

Here, Q is the raw rate of signals that are recorded at the central station. The term Q[1-h(QBER)] describes the fraction of this raw rate that remains after accounting for errors and will be referred to as the corrected key rate. Note that the binary entropy function is given by $h(e) = -e\log_2(e) - (1-e)\log_2(1-e)$. This initial implementation of our model assumes an ideal, eavesdropper-free environment. Therefore, we will evaluate and present an error-corrected rate rather than a true secret key rate.

In MDI-QKD, the raw gain Q can be calculated as follows:

$$Q_{SPS} = \frac{1}{2} \left(n \eta_t \eta_d \eta_{mem} e^{-\frac{t}{\tau_{coh}}} \right)^2. \tag{2}$$

Here, n is the number of photons (set to 1 for SPS), η_d is the detector efficiencies and η_{mem} is the total quantum memory efficiency. The term η_t represents the free-space transmittance efficiency, assuming that noise from background light sources is a negligible contribution. The modeling of the atmospheric inefficiency factors will be discussed in Section V.

Eq. 2 calculates the contribution to the total gain which accounts for the realizations that yield two clicks when both QMs herald. The expression assumes both qubits sent by Alice and Bob undergo a BSM at Charlie's intermediate station in the presence of detector (η_d) , QM (η_{mem}) and atmospheric transmittance (η_t) efficiencies. Since the QMs in

our model are assumed to be heralded, we must consider only the realizations where both qubits are loaded in the QMs. The 1/2 factor preceding each term accounts for the maximum BSM efficiency of 50%.

In order to obtain the Quantum Bit Error Rate (QBER), we must first determine the rate of incorrect bits. Because our scheme relies on a heralded quantum memory system, it is resistant to errors from detector dark counts but remains vulnerable to errors generated by the memories themselves. We utilize a simplified model in which we assume a static memory error rate [21] for both Alice's and Bob's memories, denoted as e_{mem} . The total error for the two quantum memories is therefore calculated as:

$$e_{mem} = 2E_{A/B}(1 - E_{A/B}),$$
 (3)

where $E_{A/B}$ is the error value caused by each QM in the setup. The factor of 2 accounts for the fact there are two memories in the system. The QBER then is calculated as

$$QBER = \frac{2E_{A/B}(1 - E_{A/B})}{Q},$$
 (4)

B. Rates using weak coherent pulses

The previous model describes the use of SPS, but ideal single-photon sources have not yet reached the technological maturity for widespread, practical implementation. Therefore, many real-world implementations turn to the more feasible and cheaper option of WCP which are readily available from a laser source.

Pulses composed of WCP have a Poissonian distribution of photon number states. More specifically, the number of photons per pulse is a random variable with a distribution of probabilities to contain zero, one, or more than one photon. By applying the Poisson distribution, the probability of photons in a WCP present in the QM at Charlie's station can be modeled as,

$$P_{\mu} = 1 - e^{-\mu\eta_d\eta_{mem}\eta_t},\tag{5}$$

where μ is the mean photon number per pulse. Note that Eq. 5 can be explained by unity minus the probability that a photon does not exist. Therefore, Eq. 2 will be modified as:

$$Q_{WCP} = \frac{1}{2} \left(1 - e^{-\mu \eta_t \eta_d \eta_{mem} e^{-t/\tau_{coh}}} \right)^2 \tag{6}$$

The above expression is now used with Eq. 4 and Eq. 1 to calculate the corrected key rate.

For a scaled rate, we assume repetition times that coincide with the total transmission distance between communicating parties such that $\nu=v/L$ then

$$R_{total} = \nu \cdot R_{corr}.$$
 (7)

While the utilization of WCP offers an ease of implementation, it comes with its own set of considerations and security risks. The presence of one or more photons in each pulse is not guaranteed, resulting in a probability of no photons being emitted from the sources which reduces the rate. However, if

more than a single photon is in a given pulse, the protocol is now prone to photon-number-splitting (PNS) attacks. This type of attack allows potential eavesdroppers to go undetected while obtaining information about the key by optically splitting and measuring multi-photon pulses. By siphoning off parts of the pulse while the remainder of the state still reaches the receiver, Alice and Bob will have no way of detecting Eve. To protect against PNS attacks, implementations have employed decoy states [22]. In MDI-QKD [23], by preparing WCP with a set of state amplitudes (ie. different values of mean photon number μ), channel exposure to PNS attacks will translate to yields and error rates that are inconsistent with expected values. Hence, Eve's presence can be detected.

IV. STOCHASTIC MODELING OF MDI-QKD SYSTEMS

We now turn our attention to developing a stochastic model that will allow us to predict the key rates in a MA-MDI-QKD system. With the rapid development of quantum networks, there has been much interest in the generation of predictive models for these networks. This includes modeling rates in BB84 systems and entanglement based systems [24]. Further studies have modeled networks through the development of software packages based on stochastic techniques. These packages have been used to model QKD for BB84 [25], [26] and entanglement based distribution networks [27], [28]. To date, there are limited reports on simulation methods in MDI-QKD schemes [29].

Here, we aim to develop a model logistically designed around a simplistic iterative process of QM sampling. The method allows for a robust statistical assessment of recording a successful BSM event and the corresponding key generation rate. Such predictions in real-world conditions have become increasingly important in the advancement of city-based quantum networks [30]–[32].

The primary goal is to develop a stochastic model for the prediction of MA-MDI-QKD rates over metropolitan distances. Specifically, our model aims to leverage the advantages of a MA-MDI-QKD system by allowing for asynchronous arrival of the photonic states coming from each of Alice and Bob. In this way, we incorporate the QM coherence time and our model will tabulate successful BSM events in realizations where one state has been stored in a QM for a period of time before the second arrives. We base our model on what will be called a global/local clock scheme, the logic of which is depicted in Fig. 2.

We consider the scenarios of BSM that result from both synchronous and asynchronous arrival of the photons. To simulate the probabilistic nature of QM parameters in our MA-MDI-QKD system, we employ Monte Carlo techniques for the parameters of QM efficiency and coherence time. This method tracks the journey of each photonic state starting from its source emission and transmission through free-space channels while accounting for losses and atmospheric effects, until its arrival at the central station. Once arrived at the central Bell State Measurement system, the model will obtain statistics of the QM efficiency through Monte Carlo sampling. This determines if a successful QM operation, inclusive of

storage and retrieval, has occurred for each trial. Here, we treat the QM to be heralding, that is, once a qubit has been successfully loaded in the QM it sends a message back to the party informing them of the success. The process of a QM heralding a successful qubit capture to a party and receiving a confirmation message back is recorded as a single global clock unit, equal to the transmission time, t = L/v.

In the synchronous arrival scenario, a Monte Carlo simulation samples the successful loading of qubits into each QM. The heralding from this loading is then used to inform Alice and Bob that the qubits are loaded and a return message is sent by the party to signal a BSM. During this time period, both qubits in the loaded QMs undergo lifetime decay. For this case, the global clock will always hold a value of a single unit for each success recorded.

In the case of asynchronous arrival, the QM herald informs Alice or Bob that their particular qubit was not loaded, prompting the respective party to resend their qubit. During this time, the model simultaneously models QM decay in the successful channel through Monte Carlo sampling. Each time a quantum memory (QM) successfully holds a qubit, its local clock time increases by one unit. If a QM ever needs to be reloaded with a qubit, its local clock is reset, but the global clock time for each trial will increase with each qubit sent. This process is repeated until one of two results is obtained: a qubit is successfully present in each of the two QMs, resulting in a delayed successful BSM result; or both QMs concurrently do not hold a qubit and the trial is recorded as a failure.

Once a result is obtained, the model resets and attempts another trial. After many trials, the sum of all successful trials (both instant and delayed) can be used to provide an estimation of the total gain Q. An interesting feature of our model is that it tabulates all possible records of BSM, including those that occur from photonic states arriving at their respective QMs asynchronously along with the corresponding global clock time for that trial. A system level diagram of our model is shown in Fig. 2.

This global/local clock system can also be extended for use in entanglement-based distribution systems, in a similar fashion to what has been demonstrated in other software [28].

V. METROPOLITAN FREE SPACE MA-MDI-QKD SETUP

We set out for our model to simulate MA-MDI-QKD distribution rates in an urban environment where, for example, Alice and Bob are situated on high-rise rooftops and Charlie's central node is located on another roof top between the two parties. Where his node contains a polarization based BSM composed of a 50/50 beam splitter, two polarization beam splitters, and 4 single photon detectors. In this example, our model accounts for deterministic losses of atmospheric distance, beam divergence and geometric losses and the efficiency of the collection optics at Charlie's station. These factors, in combination with the stochastic parameters of the QM, collectively determine the total gain quantum bit error rates. A schematic diagram of this setup is shown in Fig. 3.

When designing a free-space MA-MDI-QKD setup over metropolitan distances, several factors require consideration.

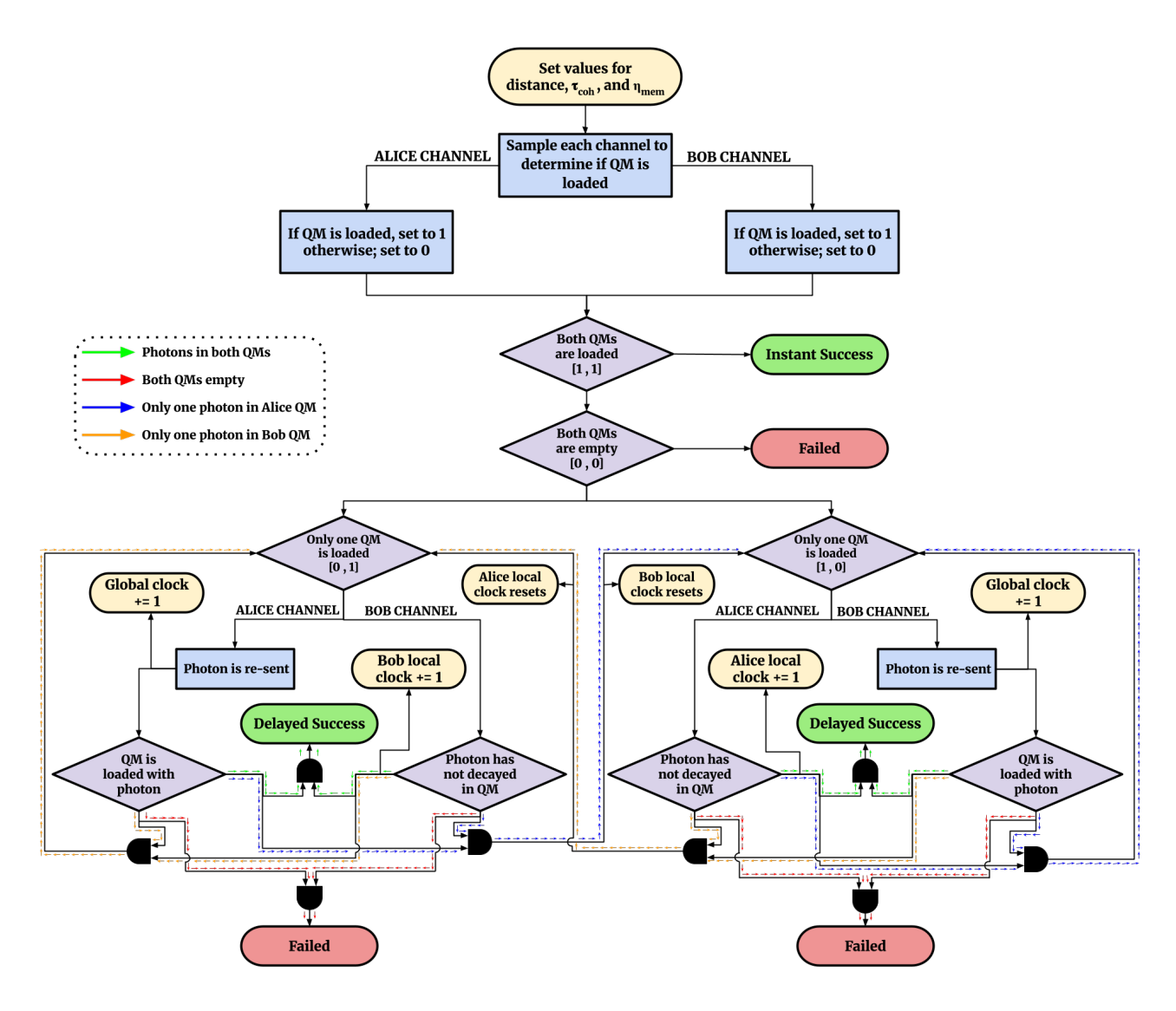


Fig. 2. Logic flow for the stochastic modeling of MA-MDI-QKD key-rates, utilizing the global/local clock scheme.

Here, we will describe the most pertinent of ones that were included in this first demonstration of our simulation model.

A. Field-deployable quantum memory system

Setting up central stations in a metropolitan environment will necessitate the availability of numerous, field-deployable QM devices. Ensemble-based QMs, such as warm vapor memories can potentially fulfill these conditions [33]. These systems have experienced a resurgence in interest in recent years. Alkali atom-based warm vapor memories, leveraging the phenomenon of Electromagnetically Induced Transparency [34] and Raman memory schemes [35], offer a system capable of the read-in and read-out operations when for storing quantum light states [36], [37]. Warm vapor memories have now reported efficiencies up to 94% [38], and, despite thermal motion, have shown coherence times of up to 1 ms [39] along with fast repetition rates [40]. Furthermore, they have shown capable of heralding in Raman schemes [41] and are moving toward the same functionality in EIT systems [42]. The relative simplicity and scalability of these warm vapour systems make them highly appealing for real-world quantum network applications [39], [43], as they do not require cryogenic cooling or complex vacuum systems often associated with other memory platforms [44]. These QM storage schemes facilitate the coherent mapping of a photonic quantum state onto the collective state of the atomic ensembles. The ondemand storage and retrieval is the functionality needed for synchronizing probabilistic qubit sources. The QMs are buffers at the central node in a MA-MDI-QKD system and serve to mitigate independent losses occurring in Alice and Bob's quantum channels.

Here we assume that both Alice and Bob's QMs operate identically and store and release photonic qubits in the same spectral mode and temporal profile. In this demonstration of our model, we assume the errors in the protocol stem from the QMs. In other words, the polarization states of Alice and Bob's qubits have a finite probability of undergoing an error due to being held in the QM. Here, we take a QM error probability of $E_{A/B}=1$ e-8. In line with the choice of a QM based on alkali vapor, we will assume a QM-compatible wavelength for

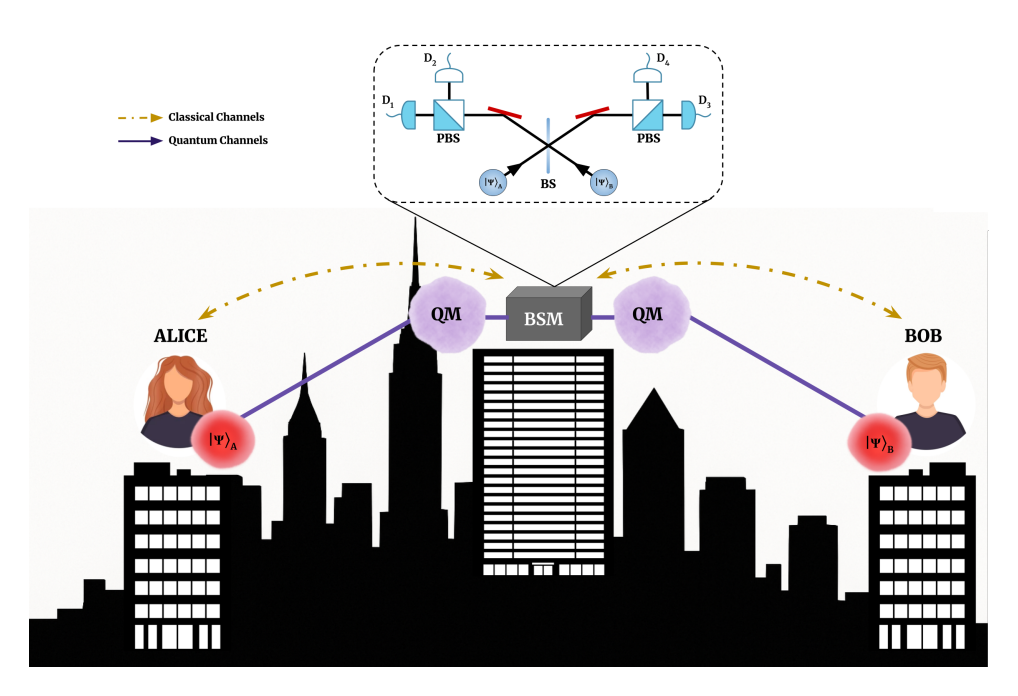


Fig. 3. Schematic of intra-city quantum communications using QKD. Parties of Alice and Bob hold qubit states at their stations situated on metropolitan rooftops. Similarly, Charlie's untrusted central node is on an intermediate rooftop hosting a polarization based BSM apparatus consisting of a beamsplitter (BS), two polarization beam splitters (PBS) and four single photon detectors D_{1-4} . Quantum channels are for qubit transmission and classical channels are for exchanging basis choices and notification of a successful BSM.

transmission at 780 nm. Beam divergence calculations will also be based on this wavelength.

B. Atmospheric loss considerations

A majority of real-world QKD demonstrations have utilized a fibre-based system [13]. Fibre waveguides provide a direct transmitter to receiver channel, an inherent single mode and being able to leverage already established metropolitan communication infrastructures. However, modeling a system designed to operate in free space requires a different set of considerations.

Detrimental effects include optical beam wander from its intended path [17], beam divergence and atmospheric absorption [45]. These phenomena not only increase loss but can also induce polarization rotation in the transmitted photons, directly affecting the fidelity of the encoded quantum states.

For our simulations and in line with other models, we use an atmospheric loss value of $\alpha_{atm\ loss}=0.1$ dB/km. The geometric loss term $T_{geo}(L)$ accounts for the reduction in received power as a function of the propagation distance L, and is dependent on the transmitting wavelength λ , beam waist ω_0 and receiver's aperture D. In our simulations, we chose values of $\lambda=780$ nm, $\omega_0=3$ mm and receiver's aperture D=0.1 m and optical collection $\eta_{coll}=0.7$ which can be reachable using adaptive optics [18]. The full channel transmission for a given length L is then given by $\eta_t(L)=\eta_{geo}(L)\eta_{coll}10^{-\alpha_{atm\ loss}L/10}.$

C. Quantum light source: single photons and weak coherent pulses

In the generation of a secret key within a MA-MDI-QKD system, the ideal scenario involves the use of true single

photons. These intrinsically provide unconditional security [1], as each detected photon definitively corresponds to a single transmitted quantum state, and are robust against PNS attacks by a potential eavesdropper. However, practical and high-rate single-photon sources remain technologically challenging and even more so in the context of a memory assisted system. As now there is an added requirement of the single photons having photonic modes (central frequency, bandwidth, polarization etc.) compatible with the QMs [46] implemented at the central station.

Hence, many experimental MDI-QKD implementations often rely on WCP. While easier to produce, WCP inherently contains a non-zero probability of emitting multiple photons per pulse. This multi-photon component opens a vulnerability to PNS attacks, where an eavesdropper can passively split off "extra" photons from a multi-photon pulse without disturbing the remaining photons [47]. To counteract this security loophole and allow for a secure key generation from WCP, decoy state protocols become indispensable [22]. By randomly varying the intensity of the WCP (sending different "decoy states" in addition to the "signal state"), the legitimate parties can effectively estimate the upper bound of information an eavesdropper could gain from multi-photon pulses, thereby allowing a secure key to be distilled from the single-photon component.

We will use WCP as a benchmark to analyze achievable distribution rates. This will provide a comparative analysis of the channel's performance without the use of a decoy state protocol, thus our simulations will yield raw error corrected key rates rather than a true secret key rate.

D. Bell state measurement apparatus

For systems utilizing polarized photons in the BSMs at the central station, active compensation or robust encoding schemes may be required to mitigate polarization distortions and rotations during transmission [48]. Furthermore, imperfect devices in a polarization-based BSM apparatus introduce significant modeling imperfections by causing a deviation from ideal behavior [49]. First is polarization misalignment or rotation which can occur from imperfect wave plates and non-ideal fiber coupling (if used). Second is mode mismatch which takes the form of time-jitter, spectral mismatch between Alice's and Bob's photons or imperfect fidelities between Alice and Bob's quantum states. They can also be introduced by the presence of any fluctuations in the brightness of Alice and Bob's qubit sources. Lastly, imperfections in the beam splitters at the central node itself can lead to improper measurement correlations. These imperfections collectively complicate the system model, requiring a more careful treatment for the BSM's efficiency and error rates [49].

Another major consideration are detector limitations such as dark counts and stray light. In a free space system, there will exist light from unwanted sources acting as a source of noise, especially in urban environments. Scattered sunlight during the day [31] and artificial lights at night [50] can contribute a substantial photon background, increasing the effective quantum bit error rate and reducing the achievable key rates. This may necessitate the use of narrow-band optical filters centered precisely on the transmitting states wavelength and advanced time-gating techniques at the receiver to distinguish true quantum signals from noise. Additionally, pointing, acquisition and tracking systems [17] are often utilized in these environments. These technologies ensure the precise alignment of the transmitting and receiving telescopes to maintain the optical link despite possible building vibrations or slight atmospheric shifts, which is relevant in multi-kilometer free-space paths. In our implementation, the presence of heralded QMs essentially removes the need for dark count consideration in the MDI-QKD rate analysis. However, extended noise models will go into future iterations of our model.

VI. KEY DISTRIBUTION RATES WITH SYNCHRONOUS ARRIVAL TIMES

For the first implementation of our model, we analyze the case where Alice and Bob's states are loaded into their QMs simultaneously and discard the attempt if either loading fails. In such a scheme, the model yields the shortest global clock time for a successful BSM between Alice and Bob as there we do not consider the case of waiting for the other QM to load. While this scenario is identical to a purely photonic based MDI-QKD setup with a central station, it serves as initial evaluation of our model.

In this scenario, we implement our model in a particular fashion. Since we are only considering successes for synchronous arrival, Alice and Bob send their qubits to the central station for loading into their specified QMs. Once successfully loaded, we assume the QMs are heralded and the central station will communicate back to Alice and Bob that the qubits

are stored. Upon receiving this message, Alice or Bob can then send a return message to the central node to perform the BSM. In this way, each QM is required to hold their qubits for one global clock count, which is the time it takes to travel a distance L before the BSM is carried out. The corresponding QM lifetime decay is then considered accordingly as $e^{-t/\tau_{coh}}$ in both our deterministic key rate equations and stochastic modeling.

We compare the results of our model with a direct BB84 protocol. In this scheme, no quantum memories are present, so we will model the impact of dark counts. Here, the gain is taken to be $Q_{BB84} = \eta_t \eta_d$, where η_t extends the full distance L between Alice and Bob. The corresponding QBER is $QBER_{BB84} = P_d/(Q_{BB84} + P_d)$ where P_d is the dark count probability and is assumed to be 2.5e - 4, which is in line with state of the art photon counting modules at 780 nm.

The plots shown in Figs. 4 and 5 represent the error-corrected key rates and assume the case where no eavesdropper is present. The curves show the results from our stochastic model (solid) assuming no delayed successes compared to those using the deterministic expressions (dashed) using Eqs. 2 and 6. We model this synchronous scenario for variable QM efficiencies and a fixed coherence time of $\tau_{coh}=0.25$ ms shown in Fig. 4. Similarly we plot variable coherence times with a fixed QM efficiency of $\eta_{mem}=0.5$ shown in Fig. 5. Rates are plotted for distances up to 35 km, which can be typical of the span of a greater metropolitan area.

As shown in Figs. 4 and 5, higher QM efficiencies will yield higher rates, with larger improvements observed for the case of a SPS source. This is because an ideal SPS source is highly reliable, with every photonic pulse containing a single photon by design. However, a WCP source has a non-zero probability of emitting zero photons. This means that a certain fraction of the transmitted pulses do not register a count, even if in principle the pulse could have reached the central station.

A good verification of our model is by overlaying the stochastic simulations with the deterministic expressions. The matching behavior between the two plots shows that our algorithm can model quantum network simulations reliant on probabilistic QMs suitable for urban environments.

Figures 4 and 5 show that the synchronous MA-MDI-QKD rate surpass the BB84 protocol at around 21 km for SPS and 6 km and 18 km for WCP of mean photon numbers $\mu=0.05$ and $\mu=0.7$ respectively. Simulations from our model also allow us the extract the QBER versus distance; for example, the average QBER remains below the 11% threshold for QM parameters of $\tau_{coh}=500~\mu{\rm s}$ and $\eta_{mem}=0.5$ for 20 km when using SPS and distances of 17 km for the cases of WCP of $\mu=0.7$. The bit errors in our simulations are grouped into QM related errors and the presence of an eavesdropper is not considered.

As seen in Figs. 4(b) and 5(b), using higher mean photon number (μ) values in WCP yields improved generation rates, particularly over longer distances where losses are more pronounced. However, in the special case exhibited here, the demand of a synchronous arrival time scheme can result in lower rates than a no-memory case due to the non-unity QM efficiency.

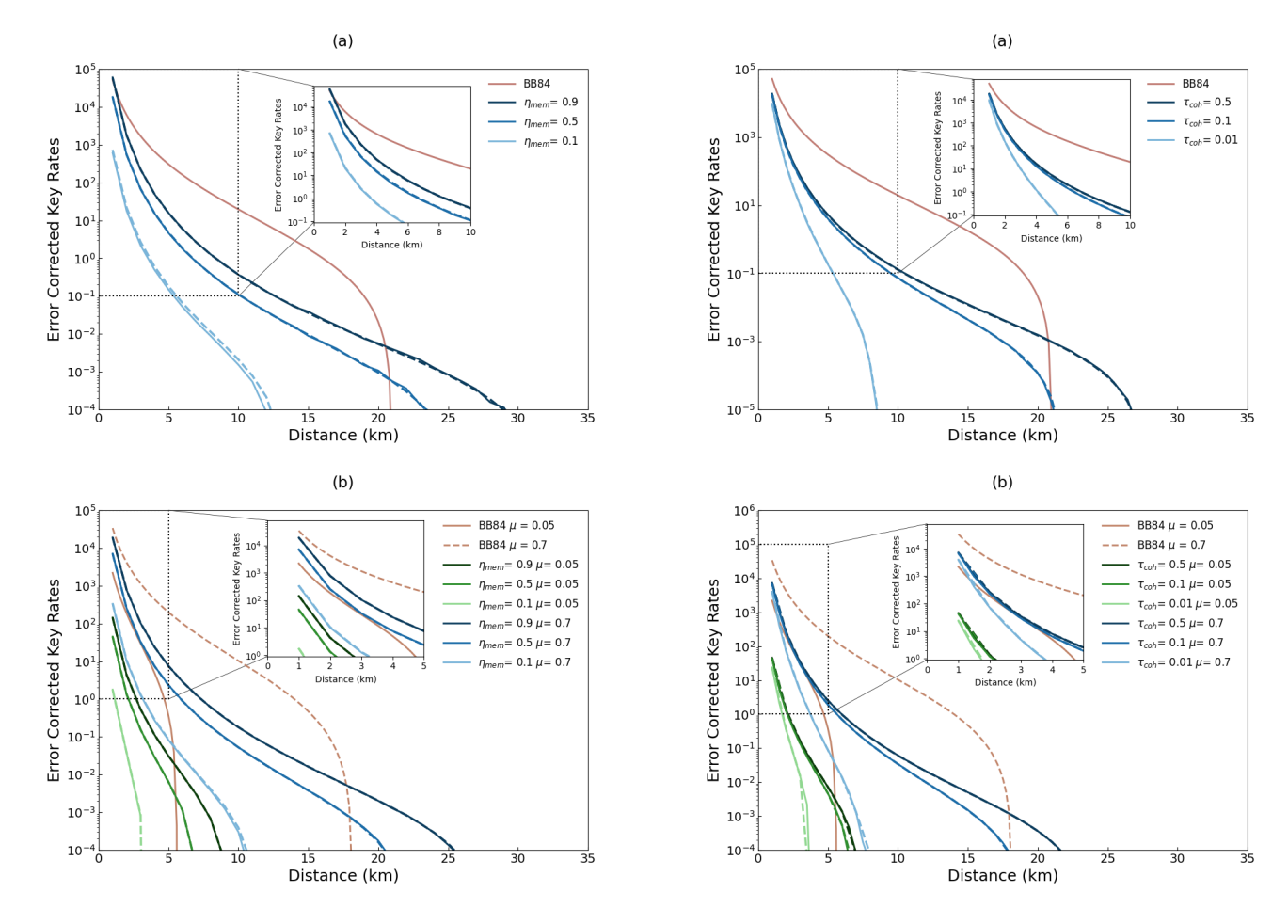


Fig. 4. (a) Error corrected key rate vs distance for distance based rates using ideal single photon source in a synchronous MA-MDI-QKD protocol with different QM efficiencies. The dashed curves correspond deterministic calculation and the solid are the corresponding results of the stochastic model. Curves represent memory efficiencies η_{mem} of 0.9, 0.5, 0.1. Distribution rate of direct BB84 is calculated with SPS. (b) Error corrected key rate vs distance for distance based rates using weak coherent pulses in a synchronous MA-MDI-QKD protocol with different QM efficiencies. The dashed curves correspond deterministic calculation and the solid are the corresponding results of the stochastic model. Curves represent a WCP of $\mu=0.7$ with QM efficiencies η_{mem} of 0.9, 0.5, 0.1 and a WCP of $\mu=0.05$ with efficiencies 0.9, 0.5, 0.1; distribution rate of direct BB84 is calculated with a WCP of $\mu=0.05$ and $\mu=0.7$.

Fig. 5. (a) Error corrected key rate vs distance for distance based rates using ideal single photon source in a synchronous MA-MDI-QKD protocol with different coherence times. The dashed curves correspond deterministic calculation and the solid are the corresponding results of the stochastic model. Curves represent coherence times τ_{coh} of 0.5 ms, 0.1 ms, 0.01 ms. Distribution rate of direct BB84 is calculated with SPS. (b) Error corrected key rate vs distance for distance based rates using weak coherent pulses in a synchronous MA-MDI-QKD protocol with different coherence times. The dashed curves correspond deterministic calculation and the solid are the corresponding results of the stochastic model. Curves represent a WCP of $\mu=0.7$ with coherence times τ_{coh} of 0.5 ms, 0.1 ms, 0.01 ms and a WCP of $\mu=0.05$ with coherence times 0.5 ms, 0.1 ms, 0.01 ms (distribution rate of direct BB84 is calculated with a WCP of $\mu=0.05$ and $\mu=0.7$.

This preliminary demonstration of our simulation algorithm shows its value as a tool for predicting the performance of MA-MDI-QKD network topologies. This model can be extended as the primary function of MA-MDI-QKD schemes is the utilization of the intermediate node to serve as a hub for numerous solitary parties.

VII. KEY RATE DISTRIBUTION WITH ASYNCHRONOUS ARRIVAL TIMES

We now turn our analysis to a setup identical to the one described in the previous section, but with Alice and Bob's transmission channels and dedicated QMs capable of asynchronous operation. Again, we assume trusted operating conditions with no eavesdropper present. Here, we now consider delayed arrival times in addition to the synchronous ones. Successful key generation events are tabulated using the

global/local clock scheme detailed in Section IV. Alice and Bob send their qubits to the central station for loading into their specified QMs which are heralded. We now remove the demand of synchronous arrival time, therefore upon Alice and Bob receiving notification of the herald from the QM, they can choose whether or not to resend their qubit. Once confirmation that both QMs possess a qubit, the scheme can undergo a BSM. The corresponding lifetime of the QM holding a qubit is stochastically modeled while waiting for the arrival of a qubit in the other channel. Successes are recorded according to a BSM measurement after successful arrival of a qubit in both channels has been confirmed. Additionally, for each success, the global clock time is also recorded when both QMs have been loaded. The scheme fails when, at any time, neither Alice or Bob's QM, holds a photon, and the algorithm shown in Fig. 2 restarts.

The error corrected rate is now modified to take into account the mean global clock time for all tabulated successes. For a particular distance L our algorithm will calculate the mean number of global clock units $\langle m \rangle$. With this modification Eq. 7 becomes

$$R_{total} = \frac{\nu}{\langle m \rangle} \cdot R_{corr}. \tag{8}$$

In Figs. 6 and 7, to highlight the results of the stochastic modeling, we plot the results of asynchronous arrival times against the a curve showing Q and QBER with an idealized $e^{-\alpha L/2}$ dependence to serve as a guide for the stochastic behavior. Fig. 6 shows the error corrected rates for a fixed QM coherence time of $\tau_{coh}=0.25$ ms and varying QM efficiency, and Fig. 7 for a fixed QM efficiency $\eta_{mem}=0.5$ and variable coherence times. Rates are shown for distances up to 50 km.

In an asynchronous setup, the mean global clock time time required for a successful BSM is longer than in a synchronous scenario since overall, the attempt frequency is reduced due to Alice and Bob possibly resending their qubits. This longer waiting period puts a stricter demand on the QMs holding a qubit.

An interesting feature of our asynchronous stochastic model is that we can see in Fig. 6, our stochastic model outperforms the model that only counts synchronous cases but with a $e^{-\alpha L/2}$ distance dependence at the low memory efficiencies for both SPS and WCP. This difference can be attributed to the lower demand for asynchronous arrival compared to synchronous. This outperformance in rate then decreases with higher memory efficiencies due to the averaging over the global clock time that occurs with the longer distances. Extracting the QBER values versus distance, the QBER remains below the 11% threshold for QM parameters of $\tau_{coh}=100~\mu s$ and $\eta_{mem}=0.5$ of 59 km when using SPS and distances of 52 km for the case of WCP with $\mu=0.7$.

Note that the asynchronous error corrected rate degrades at a reduced slope than the synchronous scheme. This can be attributed to the L/2 reduction in transmission distance needed by each Alice and Bob and the corresponding $\sim \sqrt{\eta_t}$ increase in transmission probability. Comparison between the synchronous and asynchronous scenarios Figs. 4 vs. 6 and Figs. 5 vs. 7 directly shows this impact. At a common metropolitan distance of 25 km, the asynchronous case shows an enhancement of 10^3 compared to the synchronous case.

To quantify the spread in retrieval times captured by our algorithm, Fig. 8 shows the mean global clock time against transmission distance. Also shown is the corresponding standard deviation times for each QM coherence time. As the Figure shows, longer QM coherence times translate to standard deviations in global clock time. For the lowest coherence time of 0.01 ms, variations in global clock time are non-existent after about 20 km. This makes sense as at these longer distances and short coherence times we would not expect the QM to be still holding a qubit and only instant successes are tabulated. On the contrary, for the longest coherence time shown of 0.5 ms, the longer distances, and therefore QM hold times, result in a larger variability with global clock time standard deviations range of about 0.08-0.40 ms.

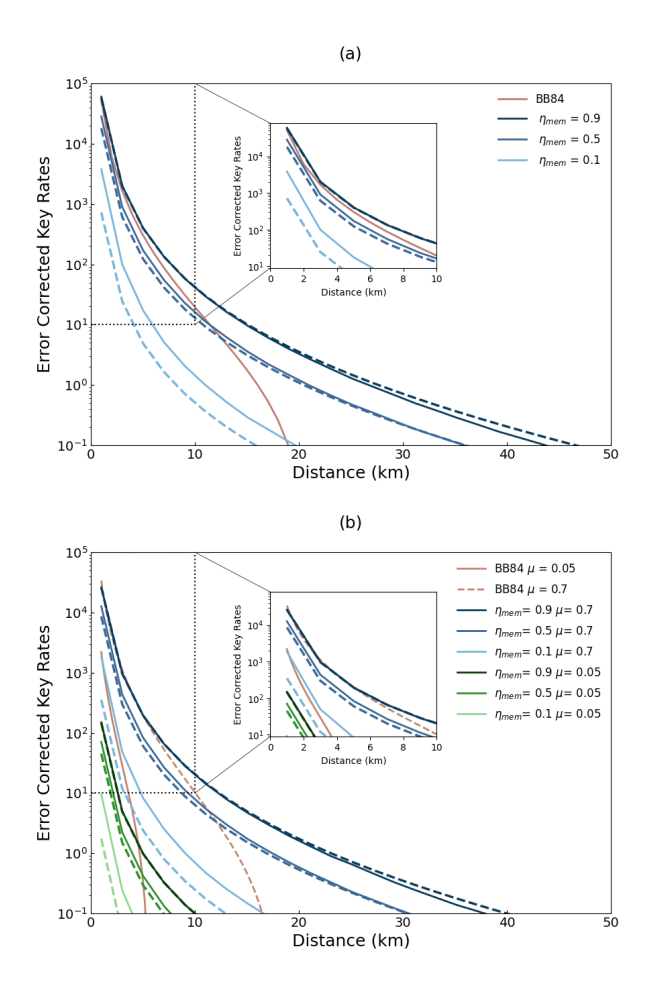
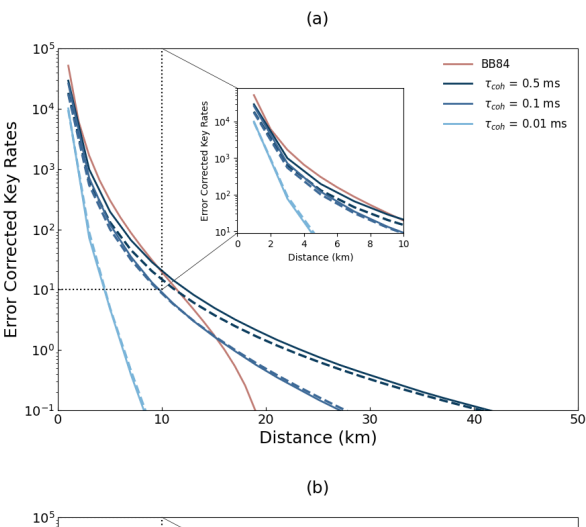


Fig. 6. Deterministic & stochastic MA-MDI-QKD vs BB84 modelling. (a) Error corrected rate vs distance for distance based rates using ideal single photon source in an asynchronous MA-MDI-QKD protocol with different QM efficiencies. The dashed curves correspond a simplified model for synchronous cases with a $e^{-\alpha L/2}$ dependence and the solid are the corresponding results of the stochastic model. Curves represent QM efficiencies η_{mem} of 0.9, 0.5, 0.1; coherence time au_{coh} kept constant at 0.25 ms. Distribution rate of direct BB84 is calculated with SPS. (b) Error corrected key rate vs distance for distance based rates using a source of weak coherent pulses in an asynchronous MA-MDI-QKD protocol with different QM efficiencies. The dashed curves correspond a simplified model for synchronous cases with a $e^{-\alpha L/2}$ dependence and the solid are the corresponding results of the stochastic model. Curves represent a WCP of $\mu = 0.7$ with QM efficiencies η_{mem} of 0.9, 0.5, 0.1 and a WCP of $\mu = 0.05$ with efficiencies 0.9, 0.5, 0.1; coherence times τ_{coh} kept constant at 0.25 ms. Distribution rate of direct BB84 is calculated with a WCP of $\mu = 0.05$ and $\mu = 0.7$.

The utility of our stochastic approach serves as a powerful complement to existing quantum network simulators. This model can be extended to MA-MDI-QKD topologies with multiple channels connected to a central hub that removes the need for dedicated fiber links between every party. This network will be a key step towards a metropolitan-wide quantum network infrastructure and a valuable tool for designing and optimizing quantum hardware.

VIII. FUTURE MODEL CONSIDERATIONS

Future versions of this tool can include an expanded set of modeling considerations for real-world MA-MDI-QKD systems.



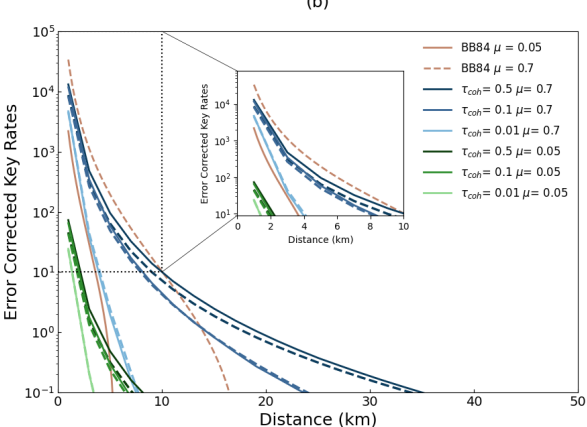


Fig. 7. Deterministic & stochastic MA-MDI-QKD vs BB84 modelling. (a) Error corrected key rate vs distance for distance based rates using ideal single photon source in a asynchronous MA-MDI-QKD protocol with different coherence times. The dashed curves correspond a simplified model for synchronous cases with a $e^{-\alpha L/2}$ dependence and the solid are the corresponding results of the stochastic model. Curves represent coherence times au_{coh} of 0.5 ms, 0.1 ms, 0.01 ms; QM efficiency η_{mem} kept constant at 0.5. Distribution rate of direct BB84 is calculated with SPS. (b) Error corrected key rate vs distance for distance based rates using weak coherent pulses in a asynchronous MA-MDI-QKD protocol with different coherence times. The dashed curves correspond a simplified model for synchronous cases with a $e^{-\alpha L/2}$ dependence and the solid are the corresponding results of the stochastic model. Curves represent a WCP of $\mu = 0.7$ with coherence times au_{coh} of 0.5 ms, 0.1 ms, 0.01 ms and a WCP of $\mu=0.05$ with coherence times 0.5 ms, 0.1 ms, 0.01 ms; QM efficiency η_{mem} kept constant at 0.5. Distribution rate of direct BB84 is calculated with a WCP of $\mu = 0.05$ and $\mu = 0.7$.

The noise models can be extended to encompass additional sources of stray light from background sunlight and urban illumination. Photons from these unwanted sources affect the MDI-QKD rate and have a direct impact on the achievable key rate [31].

Another inclusion are the detailed imperfections of effects of the BSM apparatus at the central station. Specifically, the propagation of waveplate uncertainties and beam splitter limitations on the BSM correlations [49]. This is also important as bit errors caused by an eavesdropper, Eve, are practically indistinguishable from those caused by imperfect equipment. Therefore for a thorough security analysis, all errors must be considered a result of Eve's actions.

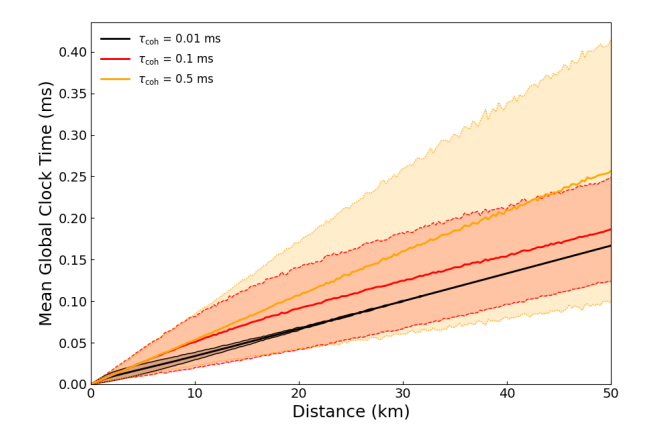


Fig. 8. Mean global clock times vs distance for coherence times τ_{coh} of 0.01 ms, 0.1 ms, 0.5 ms. The shaded area represents the spread of each plot.

A critical consideration in free space transmission systems is the effect of turbulence effects on optical field propagation. Atmospheric turbulence introduces random fluctuations in the refractive index, leading to phenomena such \vec{k} vector movement, beam divergence and scattering. These effects can severely degrade the quality of the received quantum states and have been a topic of much investigation on metropolitan scales [18]. Future model iterations would incorporate this

Finally, the work presented here assumed distribution rates using SPS and then also WCP as a rate comparison in the case of SPS being unavailable. However, when WCP are employed, a true determination of the secret key rate requires the use of decoy states [22] to safeguard against potential photon number splitting attacks. This will be investigated in future work.

IX. CONCLUSION

In this paper, we have introduced a new, simplified model specifically designed to predict the stochastic fluctuations within metropolitan-based Memory-Assisted Measurement-Device-Independent Quantum Key Distribution systems. Our approach aims to offer an easy to use tool designed to reflect real-world parameters.

Our logistical model implements a global and local clock system for each QM. This permits rate calculation for asynchronous state arrivals and the tabulation of delayed successes. With metropolitan distances in mind, loss mechanisms are based on transmission via free-space channels that include atmospheric absorption, beam divergence and collection optic efficiencies. The modeling is suited for a transmission system based on deployable QM devices such as those based on warm alkali vapours [39]. We have shown how this model provides insights into system performance under parameters including QM efficiency η_{mem} and coherence time τ_{coh} to serve as a predictive tool in practical applications.

Future work will extend modeling capabilities for modified protocols and predict performance across diverse metropolitan environments. We believe this simplified, yet powerful approach will be instrumental in advancing the design, deployment and overall understanding of future MA-MDI-QKD

networks. Furthermore, predictive modeling tools such as this are and will continue to become increasingly relevant as communication technologies progress toward global quantum networks composed of fibre, free space and satellite links [50].

REFERENCES

- [1] C. H. Bennett and G. Brassard, "Quantum cryptography: Public key distribution and coin tossing," in *Proceedings of the IEEE International Conference on Computers, Systems and Signal Processing*, vol. 560, Bangalore, India, 01 1984, pp. 175–179. [Online]. Available: https://doi.org/10.1016/j.tcs.2011.08.039
- [2] F. Xu, X. Ma, Q. Zhang, H.-K. Lo, and J.-W. Pan, "Secure quantum key distribution with realistic devices," *Rev. Mod. Phys.*, vol. 92, p. 025002, May 2020. [Online]. Available: https://link.aps.org/doi/10. 1103/RevModPhys.92.025002
- [3] H.-K. Lo, M. Curty, and B. Qi, "Measurement-device-independent quantum key distribution," *Physical Review Letters*, vol. 108, no. 13, Mar. 2012. [Online]. Available: http://dx.doi.org/10.1103/PhysRevLett. 108.130503
- [4] R. Valivarthi, I. Lucio-Martinez, P. Chan, A. Rubenok, C. John, D. Korchinski, C. Duffin, F. Marsili, V. Verma, M. D. Shaw, J. A. Stern, S. W. Nam, D. Oblak, Q. Zhou, J. A. Slater, and W. Tittel, "Measurement-device-independent quantum key distribution: from idea towards application," *Journal of Modern Optics*, vol. 62, no. 14, pp. 1141–1150, may 2015. [Online]. Available: http://dx.doi.org/10.1080/09500340.2015.1021725
- [5] A. K. Ekert, "Quantum cryptography based on bell's theorem," *Phys. Rev. Lett.*, vol. 67, pp. 661–663, Aug 1991. [Online]. Available: https://link.aps.org/doi/10.1103/PhysRevLett.67.661
- [6] A. Rubenok, J. A. Slater, P. Chan, I. Lucio-Martinez, and W. Tittel, "Real-world two-photon interference and proof-of-principle quantum key distribution immune to detector attacks," *Phys. Rev. Lett.*, vol. 111, p. 130501, Sep 2013. [Online]. Available: https://link.aps.org/doi/10. 1103/PhysRevLett.111.130501
- [7] E. Bersin, M. Grein, M. Sutula, R. Murphy, Y. Q. Huan, M. Stevens, A. Suleymanzade, C. Lee, R. Riedinger, D. J. Starling, P.-J. Stas, C. M. Knaut, N. Sinclair, D. R. Assumpcao, Y.-C. Wei, E. N. Knall, B. Machielse, D. D. Sukachev, D. S. Levonian, M. K. Bhaskar, M. Lončar, S. Hamilton, M. Lukin, D. Englund, and P. B. Dixon, "Development of a boston-area 50-km fiber quantum network testbed," *Phys. Rev. Appl.*, vol. 21, p. 014024, Jan 2024. [Online]. Available: https://link.aps.org/doi/10.1103/PhysRevApplied.21.014024
- [8] R. Valivarthi, M. G. Puigibert, Q. Zhou, G. H. Aguilar, V. B. Verma, F. Marsili, M. D. Shaw, S. W. Nam, D. Oblak, and W. Tittel, "Quantum teleportation across a metropolitan fibre network," *Nature Physics*, vol. 12, no. 11, p. 676–680, oct 2016. [Online]. Available: https://doi.org/10.1038/nphoton.2016.180
- [9] A. N. Craddock, A. Lazenby, G. B. Portmann, R. Sekelsky, M. Flament, and M. Namazi, "Automated distribution of polarizationentangled photons using deployed new york city fibers," *PRX Quantum*, vol. 5, p. 030330, Aug 2024. [Online]. Available: https://link.aps.org/doi/10.1103/PRXQuantum.5.030330
- [10] Y.-L. Tang, H.-L. Yin, Q. Zhao, H. Liu, X.-X. Sun, M.-Q. Huang, W.-J. Zhang, S.-J. Chen, L. Zhang, L.-X. You, Z. Wang, Y. Liu, C.-Y. Lu, X. Jiang, X. Ma, Q. Zhang, T.-Y. Chen, and J.-W. Pan, "Measurement-device-independent quantum key distribution over untrustful metropolitan network," *Phys. Rev. X*, vol. 6, p. 011024, Mar 2016. [Online]. Available: https://link.aps.org/doi/10.1103/PhysRevX.6. 011024
- [11] Y. Cao, Y.-H. Li, K.-X. Yang, Y.-F. Jiang, S.-L. Li, X.-L. Hu, M. Abulizi, C.-L. Li, W. Zhang, Q.-C. Sun, W.-Y. Liu, X. Jiang, S.-K. Liao, J.-G. Ren, H. Li, L. You, Z. Wang, J. Yin, C.-Y. Lu, X.-B. Wang, Q. Zhang, C.-Z. Peng, and J.-W. Pan, "Long-distance free-space measurement-device-independent quantum key distribution," *Phys. Rev. Lett.*, vol. 125, p. 260503, Dec 2020. [Online]. Available: https://link.aps.org/doi/10.1103/PhysRevLett.125.260503
- [12] M. K. Bhaskar, R. Riedinger, B. Machielse, D. S. Levonian, C. T. Nguyen, E. N. Knall, H. Park, D. Englund, M. Lončar, D. D. Sukachev, and M. D. Lukin, "Experimental demonstration of memory-enhanced quantum communication," *Nature*, vol. 580, no. 7801, p. 60–64, Mar. 2020. [Online]. Available: http://dx.doi.org/10.1038/s41586-020-2103-5

- [13] D. Bunandar, A. Lentine, C. Lee, H. Cai, C. M. Long, N. Boynton, N. Martinez, C. DeRose, C. Chen, M. Grein, D. Trotter, A. Starbuck, A. Pomerene, S. Hamilton, F. N. Wong, R. Camacho, P. Davids, J. Urayama, and D. Englund, "Metropolitan quantum key distribution with silicon photonics," *Physical Review X*, vol. 8, no. 2, Apr. 2018. [Online]. Available: http://dx.doi.org/10.1103/PhysRevX.8.021009
- [14] A. Sit, F. Bouchard, R. Fickler, J. Gagnon-Bischoff, H. Larocque, K. Heshami, D. Elser, C. Peuntinger, K. Günthner, B. Heim, C. Marquardt, G. Leuchs, R. W. Boyd, and E. Karimi, "High-dimensional intracity quantum cryptography with structured photons," *Optica*, vol. 4, no. 9, p. 1006, Aug. 2017. [Online]. Available: http://dx.doi.org/10.1364/OPTICA.4.001006
- [15] C. J. Pugh, S. Kaiser, J.-P. Bourgoin, J. Jin, N. Sultana, S. Agne, E. Anisimova, V. Makarov, E. Choi, B. L. Higgins, and T. Jennewein, "Airborne demonstration of a quantum key distribution receiver payload," *Quantum Science and Technology*, vol. 2, no. 2, p. 024009, jun 2017. [Online]. Available: https://dx.doi.org/10.1088/2058-9565/aa701f
- [16] T. Brougham and D. K. L. Oi, "Modelling efficient bb84 with applications for medium-range, terrestrial free-space qkd," *New Journal* of *Physics*, vol. 24, no. 7, p. 075002, jul 2022. [Online]. Available: https://doi.org/10.1088/1367-2630/ac7f4e
- [17] T. Jaouni, L. Scarfe, F. Bouchard, M. Krenn, K. Heshami, F. Di Colandrea, and E. Karimi, "Predicting atmospheric turbulence for secure quantum communications in free space," *Optics Express*, vol. 33, no. 5, p. 10759, Mar. 2025. [Online]. Available: http://dx.doi.org/10.1364/OE.546606
- [18] L. Scarfe, F. Hufnagel, M. F. Ferrer-Garcia, A. D'Errico, K. Heshami, and E. Karimi, "Fast adaptive optics for high-dimensional quantum communications in turbulent channels," *Communications Physics*, vol. 8, no. 1, p. 79, feb 2025. [Online]. Available: https://doi.org/10.1038/s42005-025-01986-6
- [19] O. Bel and M. Kiran, "Simulators for quantum network modelling: A comprehensive review," *Computer Networks*, vol. 263, p. 110204, may 2025. [Online]. Available: https://www.sciencedirect.com/science/article/pii/S138912862500172
- [20] G. Bebrov, "On the (relation between) efficiency and secret key rate of qkd," *Scientific Reports*, vol. 14, no. 1, p. 3638, feb 2024. [Online]. Available: https://doi.org/10.1038/s41598-024-54246-y
- [21] C. Panayi, M. Razavi, X. Ma, and N. Lütkenhaus, "Memory-assisted measurement-device-independent quantum key distribution," New Journal of Physics, vol. 16, no. 4, p. 043005, apr 2014. [Online]. Available: https://doi.org/10.1088/1367-2630/16/4/043005
- [22] X. Ma, B. Qi, Y. Zhao, and H.-K. Lo, "Practical decoy state for quantum key distribution," *Physical Review A*, vol. 72, no. 1, Jul. 2005. [Online]. Available: http://dx.doi.org/10.1103/PhysRevA.72.012326
- [23] Z. Tang, Z. Liao, F. Xu, B. Qi, L. Qian, and H.-K. Lo, "Experimental demonstration of polarization encoding measurementdevice-independent quantum key distribution," *Phys. Rev. Lett.*, vol. 112, p. 190503, May 2014. [Online]. Available: https://link.aps.org/doi/ 10.1103/PhysRevLett.112.190503
- [24] V. Scarani, H. Bechmann-Pasquinucci, N. J. Cerf, M. Dušek, N. Lütkenhaus, and M. Peev, "The security of practical quantum key distribution," *Rev. Mod. Phys.*, vol. 81, pp. 1301–1350, Sep 2009. [Online]. Available: https://link.aps.org/doi/10.1103/RevModPhys.81. 1301
- [25] O. K. Jasim, S. Abbas, E.-S. M. El-Horbaty, and A.-B. M. Salem, "Quantum key distribution: Simulation and characterizations," *Procedia Computer Science*, vol. 65, pp. 701–710, 2015. [Online]. Available: https://www.sciencedirect.com/science/article/pii/S1877050915028446
- [26] A. Kohnle and A. Rizzoli, "Interactive simulations for quantum key distribution," *European Journal of Physics*, vol. 38, no. 3, p. 035403, mar 2017. [Online]. Available: https://dx.doi.org/10.1088/1361-6404/aa62c8
- [27] X. Wu, A. Kolar, J. Chung, D. Jin, T. Zhong, R. Kettimuthu, and M. Suchara, "Sequence: a customizable discrete-event simulator of quantum networks," *Quantum Science and Technology*, vol. 6, no. 4, p. 045027, sep 2021. [Online]. Available: https://doi.org/10.1088/2058-9565/ac22f6
- [28] V. Semenenko, X. Hu, E. Figueroa, and V. Perebeinos, "Entanglement generation in a quantum network with finite quantum memory lifetime," AVS Quantum Science, vol. 4, no. 2, p. 012002, jun 2022. [Online]. Available: https://doi.org/10.1116/5.0082239
- [29] G. K. Simon, B. K. Huff, W. M. Meier, L. O. Mailloux, and L. E. Harrell, "Quantification of the impact of photon distinguishability on measurement-device-independent quantum key distribution," *Electronics*, vol. 7, no. 4, p. 49, apr 2018. [Online]. Available: https://doi.org/10.3390/electronics7040049

- [30] M. Rajpurohit, K. M. Deka, V. P. Singh, and H. P, "Advanced qkd protocols and practical challenges," in 2024 IEEE International Conference on Public Key Infrastructure and its Applications (PKIA), 2024, pp. 1–8. [Online]. Available: http://doi.org/10.1109/PKIA62599. 2024.10727858
- [31] A. Kržič, S. Sharma, C. Spiess, U. Chandrashekara, S. Töpfer, G. Sauer, L. J. González-Martín del Campo, T. Kopf, S. Petscharnig, T. Grafenauer, R. Lieger, B. Ömer, C. Pacher, R. Berlich, T. Peschel, C. Damm, S. Risse, M. Goy, D. Rieländer, A. Tünnermann, and F. Steinlechner, "Towards metropolitan free-space quantum networks," npj Quantum Information, vol. 9, no. 1, p. 95, sep 2023. [Online]. Available: https://doi.org/10.1038/s41534-023-00754-0
- [32] H. Zhang, X. Zhang, J. Eng, M. Meunier, Y. Yang, A. Ling, J. Zúñiga Pérez, and W. Gao, "Metropolitan quantum key distribution using a GaN-based room-temperature telecommunication single-photon source," *Phys. Rev. Appl.*, vol. 23, p. 054022, May 2025. [Online]. Available: https://link.aps.org/doi/10.1103/PhysRevApplied.23.054022
- [33] N. Sangouard, C. Simon, H. de Riedmatten, and N. Gisin, "Quantum repeaters based on atomic ensembles and linear optics," *Rev. Mod. Phys.*, vol. 83, pp. 33–80, Mar 2011. [Online]. Available: https://link.aps.org/doi/10.1103/RevModPhys.83.33
- [34] M. Namazi, C. Kupchak, B. Jordaan, R. Shahrokhshahi, and E. Figueroa, "Ultralow-noise room-temperature quantum memory for polarization qubits," *Phys. Rev. Appl.*, vol. 8, p. 034023, Sep 2017. [Online]. Available: https://link.aps.org/doi/10.1103/PhysRevApplied.8.034023
- [35] S. Thomas, S. Sagona-Stophel, Z. Schofield, I. Walmsley, and P. Ledingham, "Single-photon-compatible telecommunications-band quantum memory in a hot atomic gas," *Phys. Rev. Appl.*, vol. 19, p. L031005, Mar 2023. [Online]. Available: https://link.aps.org/doi/10. 1103/PhysRevApplied.19.L031005
- [36] M. D. Eisaman, A. André, F. Massou, M. Fleischhauer, A. S. Zibrov, and M. D. Lukin, "Electromagnetically induced transparency with tunable single-photon pulses," *Nature*, vol. 438, no. 7069, pp. 837–841, dec 2005. [Online]. Available: https://doi.org/10.1038/nature04327
- [37] M. Lobino, C. Kupchak, E. Figueroa, and A. I. Lvovsky, "Memory for light as a quantum process," *Physical Review Letters*, vol. 102, no. 20, May 2009. [Online]. Available: http://dx.doi.org/10.1103/PhysRevLett. 102 203601
- [38] J. Guo, Z. Wu, G. Bao, P. Yang, Y. Wu, L. Q. Chen, and W. Zhang, "Near-perfect broadband quantum memory enabled by intelligent spinwave compaction," 2025, preprint. [Online]. Available: https://arxiv.org/abs/2505.02424
- [39] Y. Wang, A. N. Craddock, R. Sekelsky, M. Flament, and M. Namazi, "Field-deployable quantum memory for quantum networking," *Phys. Rev. Appl.*, vol. 18, p. 044058, Oct 2022. [Online]. Available: https://link.aps.org/doi/10.1103/PhysRevApplied.18.044058
- [40] R. Finkelstein, E. Poem, O. Michel, O. Lahad, and O. Firstenberg, "Fast, noise-free memory for photon synchronization at room temperature," *Science Advances*, vol. 4, no. 1, p. eaap8598, jan 2018. [Online]. Available: https://doi.org/10.1126/sciadv.aap8598
- [41] P. S. Michelberger, T. F. M. Champion, M. R. Sprague, K. T. Kaczmarek, M. Barbieri, X. M. Jin, D. G. England, W. S. Kolthammer, D. J. Saunders, J. Nunn, and I. A. Walmsley, "Interfacing ghz-bandwidth heralded single photons with a warm vapour raman memory," *New Journal of Physics*, vol. 17, no. 4, p. 043006, apr 2015. [Online]. Available: https://doi.org/10.1088/1367-2630/17/4/043006
- [42] P.-J. Tsai, Y.-F. Hsiao, and Y.-C. Chen, "Quantum storage and manipulation of heralded single photons in atomic memories based on electromagnetically induced transparency," *Phys. Rev. Res.*, vol. 2, p. 033155, Jul 2020. [Online]. Available: https: //link.aps.org/doi/10.1103/PhysRevResearch.2.033155
- [43] Y. Wang, A. N. Craddock, J. M. Mendoza, R. Sekelsky, M. Flament, and M. Namazi, "High-fidelity entanglement between a telecom photon and a room-temperature quantum memory," 2025, preprint. [Online]. Available: https://arxiv.org/abs/2503.11564
- [44] C. Clausen, F. Bussières, M. Afzelius, and N. Gisin, "Quantum storage of heralded polarization qubits in birefringent and anisotropically absorbing materials," *Phys. Rev. Lett.*, vol. 108, p. 190503, May 2012. [Online]. Available: https://link.aps.org/doi/10.1103/PhysRevLett. 108.190503
- [45] A. Ajith and S. S. Veni, "Exploring satellite quantum key distribution under atmospheric constraints," aug 2025. [Online]. Available: https://arxiv.org/abs/2508.05235
- [46] A. MacRae, T. Brannan, R. Achal, and A. I. Lvovsky, "Tomography of a high-purity narrowband photon from a transient atomic collective excitation," *Phys. Rev. Lett.*, vol. 109, p. 033601, Jul 2012. [Online]. Available: https://link.aps.org/doi/10.1103/PhysRevLett.109.033601

- [47] N. Lütkenhaus and M. Jahma, "Quantum key distribution with realistic states: photon-number statistics in the photon-number splitting attack," New Journal of Physics, vol. 4, no. 1, p. 44, jul 2002. [Online]. Available: https://doi.org/10.1088/1367-2630/4/1/344
- [48] Y. Tan, J. Wang, J. Wu, and Z. He, "Real-time polarization compensation method in quantum communication based on channel muller parameters detection," *Communications Engineering*, vol. 3, no. 1, p. 57, mar 2024. [Online]. Available: https://doi.org/10.1038/s44172-024-00198-0
- [49] F. Xu, M. Curty, B. Qi, and H.-K. Lo, "Practical aspects of measurement-device-independent quantum key distribution," *New Journal of Physics*, vol. 15, no. 11, p. 113007, nov 2013. [Online]. Available: https://dx.doi.org/10.1088/1367-2630/15/11/113007
- [50] M. Yastremski, F. Hufnagel, K. B. Kuntz, L. Scarfe, T. Jaouni, T. Jennewein, E. Karimi, and H. Khabat, "Estimating the impact of light pollution on quantum communication between qeyssat and canadian quantum ground station sites," *EPJ Quantum Technology*, vol. 12, no. 1, p. 8, feb 2025. [Online]. Available: https://doi.org/10.1140/epjqt/s40507-025-00331-8